Searching for SUSY in all hadronic final states with the α_T variable

Bryn Mathias
Imperial College London

Supervisor: Dr Alex Tapper

Abstract

This is a thesis.

Declaration

There are many like it.

Author

Acknowledgements

Thanks.

Contents

Chapter 1

Introduction

The accelerator and detectors The Large Hadron Collider (LHC) [3] is a proton-proton collider which is situated in the Large Electron Positron (LEP) tunnel approximately 100 m under the franco-swiss border. Design center of mass energy is 14 TeV with an instantaneous luminosity of $1 \times 10e^{34} cm^{-2} s^{-1}$. However during 2011 the center of mass energy was 7 TeV and the maximum luminosity was $5 \times 10e^{33}$ $cm^{-2} s^{-1}$. To achieve this high energy and high beam current the LHC uses superconducting niobium-titanium magnets, cooled to a temperature of 1.8 Kelvin, that produce a maximum field strength of 8.36 Tesla.

TODO: we might well need some more stuff about the LHC its self in here!

Situated around the LHC ring are four detectors, two general detectors ATLAS [1] and CMS (see Chapter 3 for a detailed discussion of the CMS detector) [7][11] which are designed to measure the standard model to high precision and search for new physics. The LHC beauty experiment [9] is designed to study at previously unattainable precision the decays of heavy quark flavors, both to measure the standard model couplings and to search for beyond the standard model (BSM) physical processes. Finally the ALICE [2] experiment is designed to run when the LHC is running in it's secondary mode where rather than proton bunches, lead ions are collided, in an effort to study the quark-gluon plasma.

New physics Whilst the theory of the standard model and of new physics models will be discussed in chapter 2 it is prudent to discuss the observable features of these models with regard to design requirements for the general purpose detectors.

Chapter 2

Theory

Chapter 3

The CMS detector

3.1 The High Level Trigger System

Chapter 4

Offline Object Reconstruction and Identification.

4.1 Hadronic Jets.

AK5 calo jets – explanation of the jet algos. How they are clustered at CMS. No need to mention PF? (we don't use it so why bother). Energy resolution, Jet energy corrections, ID. 2011 note

4.2 Electrons.

GSF elections - ID, use tracking. Veto on elections. 2011 note

4.3 Muons.

GPT muons - exact ID's, reconstruction methods. both veto and used to collect the control sample. 2011 note

4.4 Photons.

Veto and control sample - noise and spike cleaning 2011 note

4.5 Noise cleaning.

Dead ecal sections. monsters. Trackless events. 2011 note.

Chapter 5

Level One Calorimeter Trigger

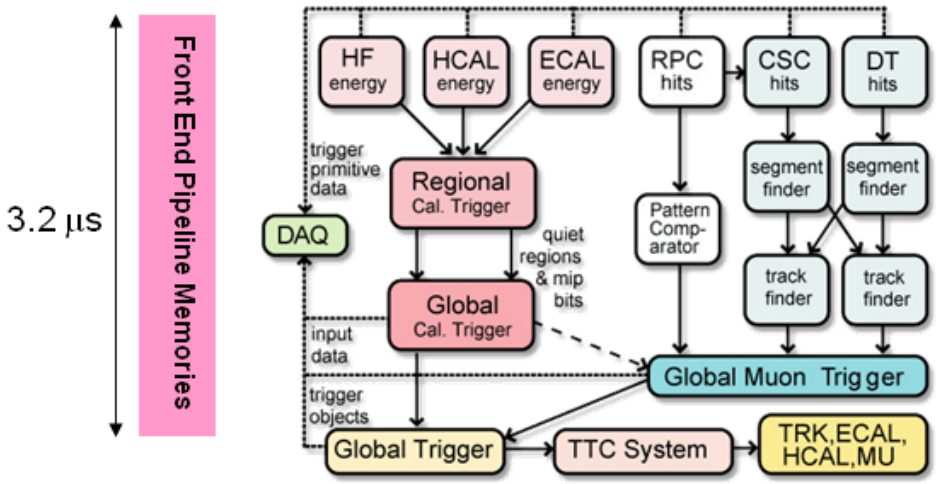

Figure 5.1: The CMS Level-1 Trigger system

The CMS Level-1 trigger system[4] is a pipelined dead-timeless system based on custom-built electronics. The Level-1 trigger is a combination of several sub systems, which are interconnected as depicted in Figure 5.1.

Corse grain information from the electro-magnetic, hadronic and forward calorimeters is processed by the Regional Calorimeter Trigger (RCT), this is then passed to the Global Calorimeter Trigger (GCT) where the corse grain information is clustered in to physics objects, these objects are then passed to the Global Trigger where the Level-1 accept decision is made. Due to the limited size of the pipe line this Level-1 accept must be issued within 4.0 μs.

The objects passed from the GCT to the GT include electro-magnetic objects, both electrons and photons as due to the lack of tracking information at the Level-1 trigger these objects are indistinguishable, jets and energy sums.

The RCT generates up to 72 isolated and non-isolated electro-magnetic objects, these are sorted by rank, which is equivalent to transverse energy E_{T}. The four highest ranked electro-magnetic objects are then passed via the GCT to the GT at an equivalent data rate of 29 Gbs^{-1} per type.

Hadronic objects under go two clustering steps. First the transverse energy sums of the ECAL and corresponding HCAL towers are calculated, the towers are then summed in to 4×4 trigger regions, these are passed to the GCT at a data rate of 172.8 Gbs^{-1}. These trigger regions are clustered in to jet candidates by the GCT and ranked. The jets are then sub-divided in the categories depending on their pseudo-rapidity and the result of τ identification.

Energy sums come in two forms, the total transverse energy E_{T} which is the scalar sum of all transverse energies and the total jet transverse energy H_{T} which is calculated as the scalar sum of all jets above some programable threshold.

The missing energy equivalents of these $\not{E}_{\mathrm{T}}$ and $\not{H}_{\mathrm{T}}$ are formed from the negative vector sum of the objects considered for the transverse sums.

5.1 Leve-1 Trigger Jet Algorithm

FIXME: This is taken pretty much straight from [8] might want to steal less??

The CMS detector can be un-rolled in the ϕ direction to form a rectangular grid of the 396 calorimeter regions, connected along the ϕ edge. The rectangle 18 ϕ divisions (from $-180° < \phi \leq 180°$) by 22 η divisions (from $-5 < \eta < 5$). Each ϕ division corresponds to 20°. The η divisions correspond to $\Delta\eta = 0.5$ in the forward calorimeters and to $\Delta\eta \approx 0.348$ in the barrel. A pictorial representation of this can be seen in figure 5.3.

A jet candidate is created if the sum of the ECAL and HCAL energies of the central calorimeter region has an energy deposit larger than all of its neighbours, as shown in figure 5.2 The jet is centered at this region where $p_T^{central} > p_T^{surrounding}$ and the transverse energies of the surrounding regions are summed in to the central region. The jet is then

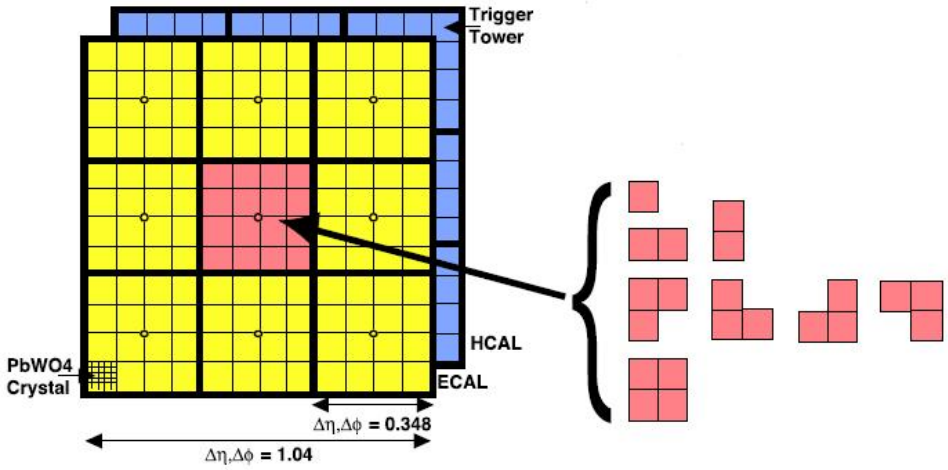

Figure 5.2: The 3 × 3 jet-finder window at Level-1. Each cell represents a trigger tower, which is the sum of the HCAL and ECAL transverse energies. The τ-jet veto patterns are shown to the right.

classified as a τ jet if $|\eta| < 3.0$ and none of the τ veto bits are set. If any τ vetoes are set the jet is classified as a central jet. The jet is classified as forward if $3.0 < |\eta| < 5.0$

The τ-vetoes are set by the RCT depending on whether or not the energy depositions in up to four contiguous trigger towers are below a programmable fraction of the regional E_{T} as shown in Figure 5.2.

It is possible to apply separate jet energy corrections to each of the sub categories of GCT jets. These corrections are discussed in detail in Section 5.2

In order to reduce the total data duplicated and shared between the jet finders the GCT employs a pre-clustering algorithm, which involves 18 jet finders operating simultaneously over the whole detector. These jet finders then only share information with neighbouring regions when the clustered jets are found. Figure 5.3 shows the boundaries between which the jet finders operate, these map naturally on to one RCT crate per jet finder. A maximum of 3 jets can be found on each of the ϕ strips acted on by the jet finders, this gives a maximum of 108 jets per event. In order to preserve continuity across the $\eta = 0$ boundary, the two adjacent trigger regions are shared between the jet finders.

An example of the jet finding is shown in Figure 5.4. The first step is to create a 2×3 mini cluster around any local maxima found in the 12×2 strip. Equality statements are imposed so that the central cell is greater than its neighbours in some directions and

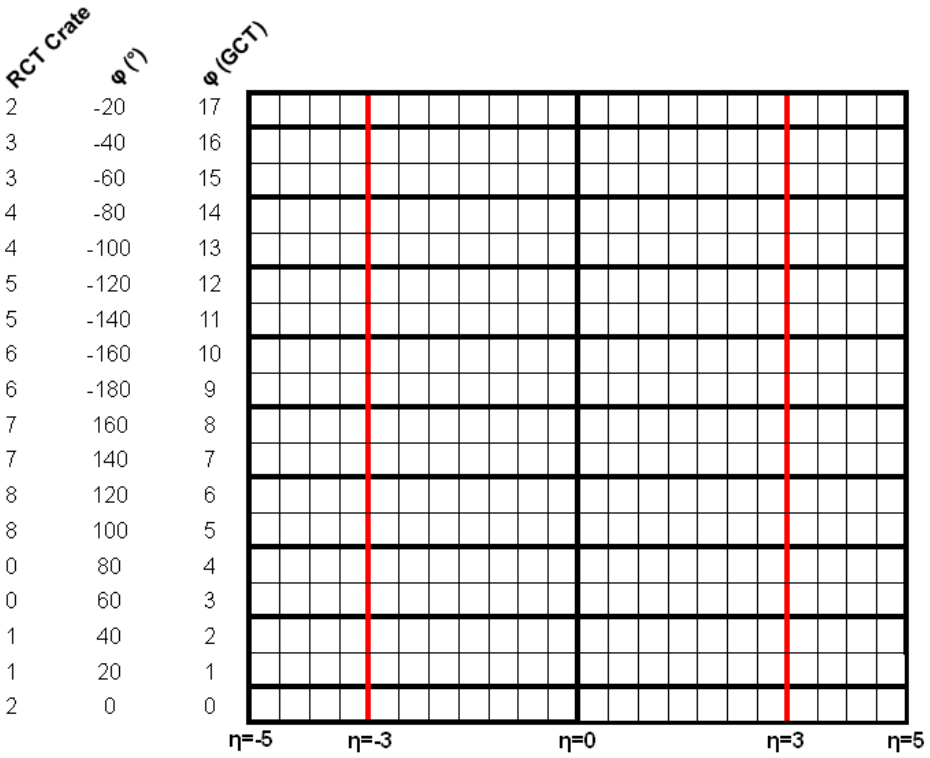

Figure 5.3: The calorimeter map that the 3 × 3 jet-finder operates over is made up for 396 calorimeter regions, each jet finder is mapped on to an RCT crate which is composed of an 11 × 2 strip of these regions. RCT crate labels are shown for negative η only.

greater than or equal to the neighbours other directions to enforce a gap of at least one trigger region in both η and ϕ between the centres of the clustered jets.

In the second step the jet finder transfers the three largest mini clusters on a given ϕ strip to the closest ϕ strip on the neighbouring jet finder. These are then compared against the existing mini clusters in that ϕ strip, those that are adjacent or diagonally adjacent to a larger mini cluster are removed. The inequalities statements are then reimposed to prevent problems with clusters having the same energies. In the final stages the mini clusters have their three adjacent regions summed in to produce a 3 × 3 jet cluster. Finally the four highest ranked jets are corrected and passed to the GT.

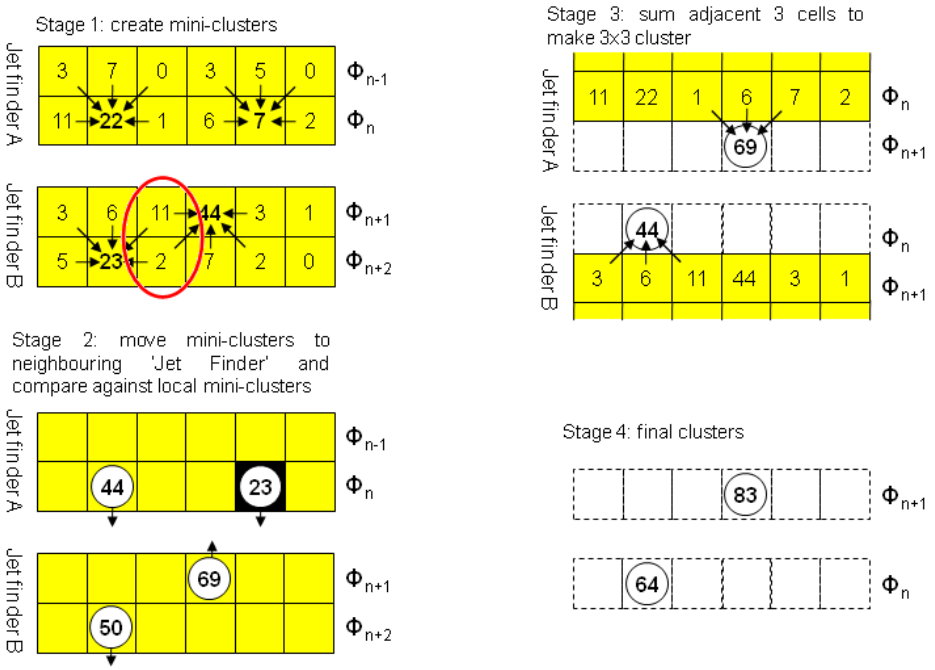

Figure 5.4: The Level-1 jet clustering method, six cells in η are shown. An example of overlapping jets is shown

5.2 Level-1 Trigger Performance

FIXME: Can i just copy the stuff out of the L1 performance note here for the corrections? I will need to re-make a bunch of the plots though :(Jobs set running as of 24th july – jobs are finally complete.

Each offline jet is matched to a Level-1 trigger jet with the smallest δR, for a match to be considered good $\delta R < 0.5$ is required. The δR distribution is show in Figure 5.5. The energy of the leading offline matched jet is then recorded to form the denominator. To form the numerator the Level-1 jet that the offline jet is matched to is required to have an energy above some desired threshold.

To compare the performance of each of the triggers each of the turn on curves are fitted with an error function. Three example single object triggers are tested these are; L1_SingleJet16, L1_SingleJet36 and L1_SingleJet52, where the number refers to the requested E_{T} threshold.

The performance is measured under two different pile up conditions, the first is where the mean number of interactions per bunch crossing ($< PU >$) is less than 16. The events studied are taken with a single μ HLT trigger namely HLT_IsoMu24 which requires

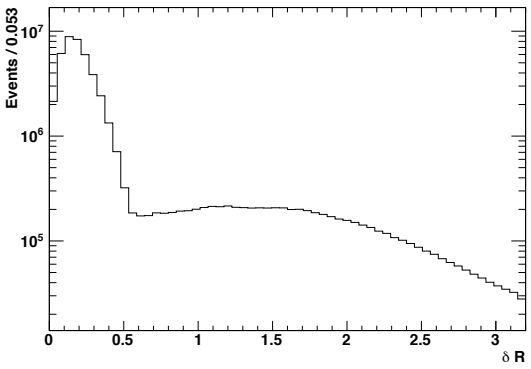

Figure 5.5: δR distribution before any selection cut, matching Level-1 jets to offline jets.

there to be at least one muon with $p_{\mathrm{T}} \geq 24$ GeV passing loose isolation, this removes any biases on the turn on from pre selecting with a hadronic trigger. To test the performance of the trigger system under high pile up conditions ($< PU > \leq 32$) a dedicated high pile up fill of the LHC was performed.The high pile up fill is studied from two points of view, the first is with regard to standard anti-k$_t$(0.5) calorimeter jets. Secondly the performance is measured against anti-k$_t$(0.5) calorimeter jets that are corrected for pile up.

Figure 5.6 shows the performance of the three example Level-1 single jet triggers with the fit results listed in Table 5.1. Figure 5.7 shows the performance of the same three triggers during high pile up conditions when compared to pile up corrected anti-k$_t$(0.5) calorimeter jets. This should be compared with Figure 5.8 where the anti-k$_t$(0.5) calorimeter jets are not corrected for pile up. The fit results for these two sets of offline conditions are listed in Table 5.2 and 5.3 respectively.

Due to the small amount of data collected in the high pile up run there are an insufficient number of events with high $\not\!\!E_{\mathrm{T}}$,$\not\!\!H_{\mathrm{T}}$ and H_{T} to measure the high pile up performance. However the performance in low pile up conditions is presented below, it is noted that as there are no HLT paths seeded by a Level-1 E_{T} trigger the performance is not measured.

Figure 5.9 shows the performance of four Level-1 H_{T} triggers with thresholds of 50, 75, 100 and 150 GeV, the fit results to each of these performance curves is detailed in Table 5.4. The shift in μ to larger values than the online Level-1 trigger threshold is due to Level-1 H_{T} being formed from the internal GCT jets before they have their energy corrected. The offline quantity is constructed using corrected anti-k$_t$(0.5) calorimeter jets

with the requirement that jets contributing to H_{T} have $E_{\mathrm{T}} \geq 40$ GeV as this definition is used when calculating HLT quantities.

Figure 5.10 shows the performance of two Level-1 $\not{H}_{\mathrm{T}}$ triggers with thresholds of 30 and 50 GeV, with the fit results listed in Table 5.5. Due to $\not{H}_{\mathrm{T}}$ being a vectorial sum, it is important to use the same objects offline and online as the addition or removal of an object from the sum has a non trivial effect on the length of the final vector, however Level-1 $\not{H}_{\mathrm{T}}$ is formed from the same objects at Level-1 H_{T}, namely uncorrected Level-1 jets with $E_{\mathrm{T}} \geq 10$ GeV. The performance is measured with respect to $\not{H}_{\mathrm{T}}$ constructed from offline anti-k$_t$(0.5) calorimeter jets with $E_{\mathrm{T}} \geq 15$ GeV.

FIXME: there will be an explanation of L1FastJet corrections somewhere, point this section to it

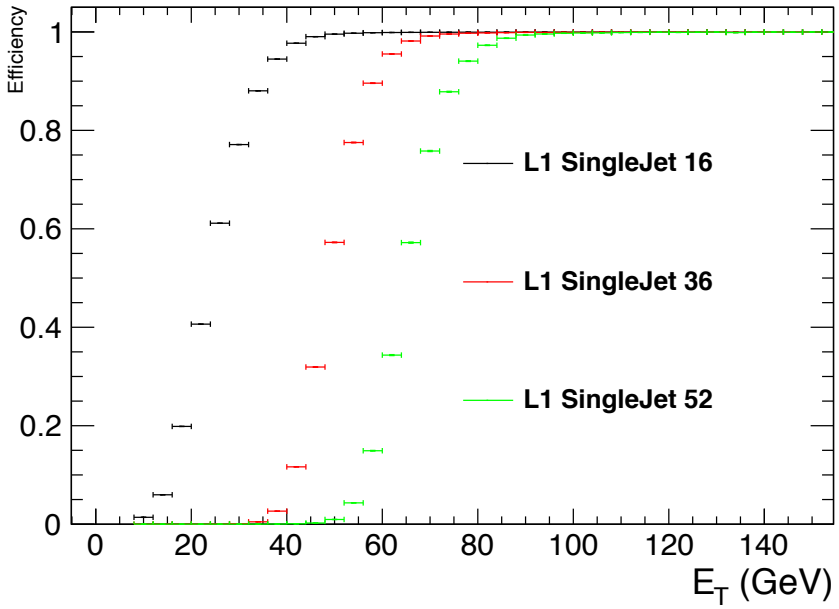

Figure 5.6: Turn on curves for three Level-1 single jet triggers, in terms of offline corrected anti-k$_t$(0.5) calorimeter jet E_{T}.

FIXME: put in the run no of the HPF in here

$$fit = \frac{\epsilon}{2} \times (1 + \frac{2}{\sqrt{\pi}} \int_0^x e^{-t^2} dt)/\sqrt{2}\sigma. \; where \; t = \epsilon - \mu \tag{5.1}$$

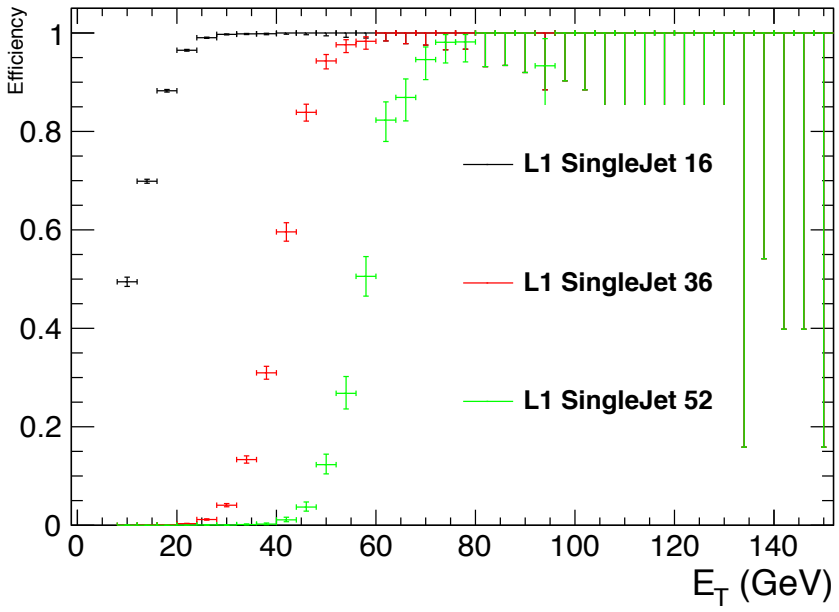

Figure 5.7: Turn on curves for the three Level-1 single jet triggers in terms of offline corrected anti-k$_t$(0.5) calorimeter jet E_{T} in high pile up conditions.

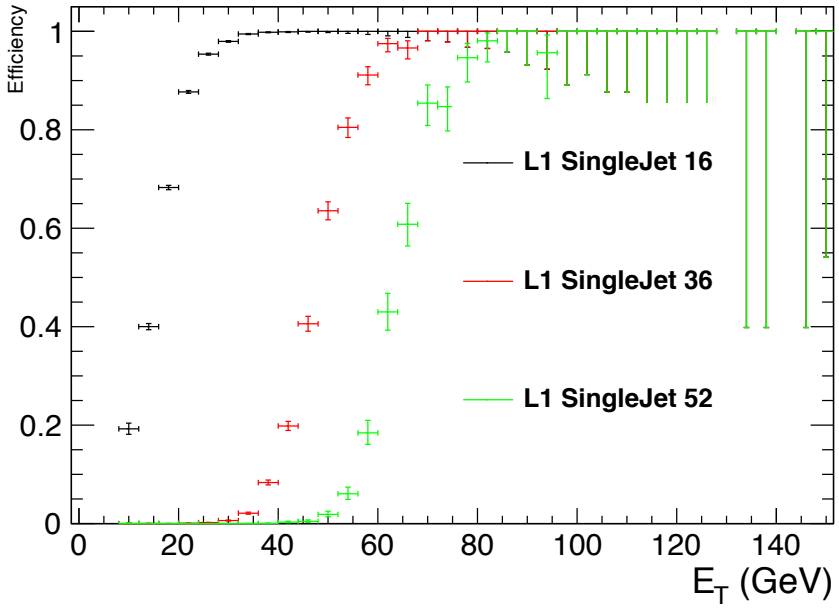

Figure 5.8: Turn on curves for the three Level-1 single jet triggers in terms of offline anti-k$_t$(0.5) calorimeter jets where the energies are corrected for energy from the pile up interactions using the FastJet correction method.

FIXME: is this even right? where σ describes the resolution, ϵ gives the maximum efficiency and μ refers to the point at which the efficiency is 50%. Throughout $\epsilon = 1.0$ is assumed.

Trigger	σ	μ
L1_SingleJet16	7.48	24.27
L1_SingleJet36	6.08	49.25
L1_SingleJet52	6.75	65.11

Table 5.1: Results of an error function fit to the turn on curves for Level-1 single jet triggers in run 2011B. Preselected on an Isolated Muon trigger.

Trigger	σ	μ
L1_SingleJet16	6.37	10.48
L1_SingleJet36	6.35	40.73
L1_SingleJet52	6.65	57.48

Table 5.2: Results of an error function fit to the turn on curves for Level-1 single jet triggers in the run 2011B high pile up fill Where offline hadronic objects are corrected for pile up using the FastJet calculation. Preselected on a zero bias trigger.

Trigger	σ	μ
L1_SingleJet16	6.07	15.20
L1_SingleJet36	7.05	47.77
L1_SingleJet52	6.74	63.68

Table 5.3: Results of an error function fit to the turn on curves for Level-1 single jet triggers in the run 2011B high pile up fill. Preselected on a zero bias trigger.

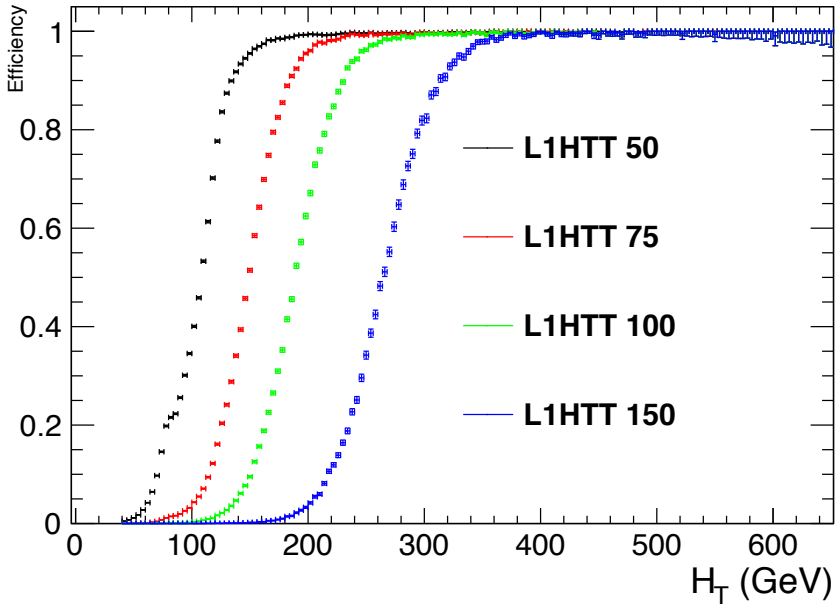

Figure 5.9: Turn on curves for the Level-1 H_T triggers. The fit results are listed in Table 5.4

Trigger	σ	μ
L1_HTT50	24.73	105.13
L1_HTT75	28.12	148.91
L1_HTT100	31.20	189.04
L1_HTT150	37.46	265.21

Table 5.4: Results of an error function fit to the turn on curves for Level-1 hadronic energy sum (H_T) triggers in run 2011B. Preselected on an Isolated Muon trigger.

Trigger	σ	μ
L1_HTM30	20.45	70.02
L1_HTM50	17.44	83.54

Table 5.5: Results of an error function fit to the turn on curves for Level-1 hadronic energy sum ($\not{H}_T$) triggers in run 2011B. Preselected on an Isolated Muon trigger.

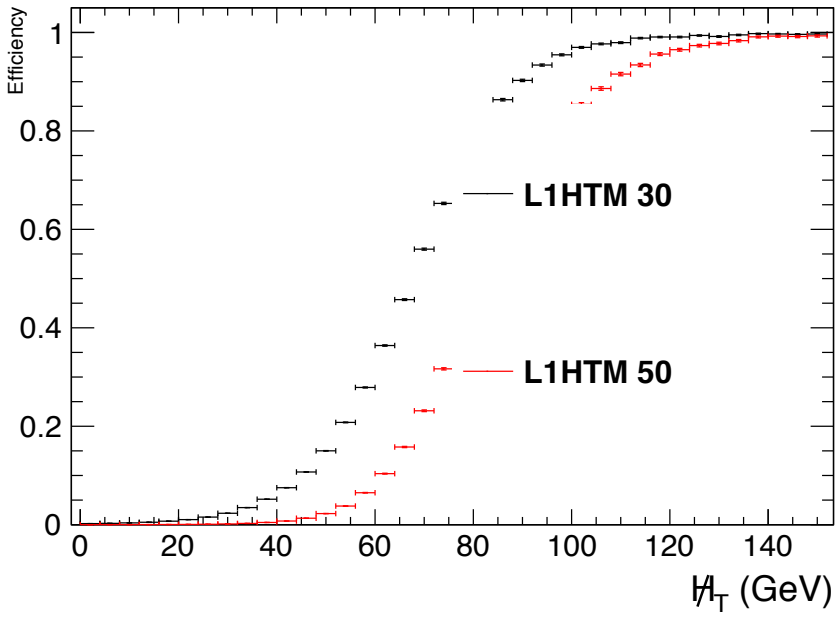

Figure 5.10: Performance of the Level-1 $\not{H}_T$ triggers, preselecting on HLT_IsoMu24. The fit results are listed in Table 5.5.

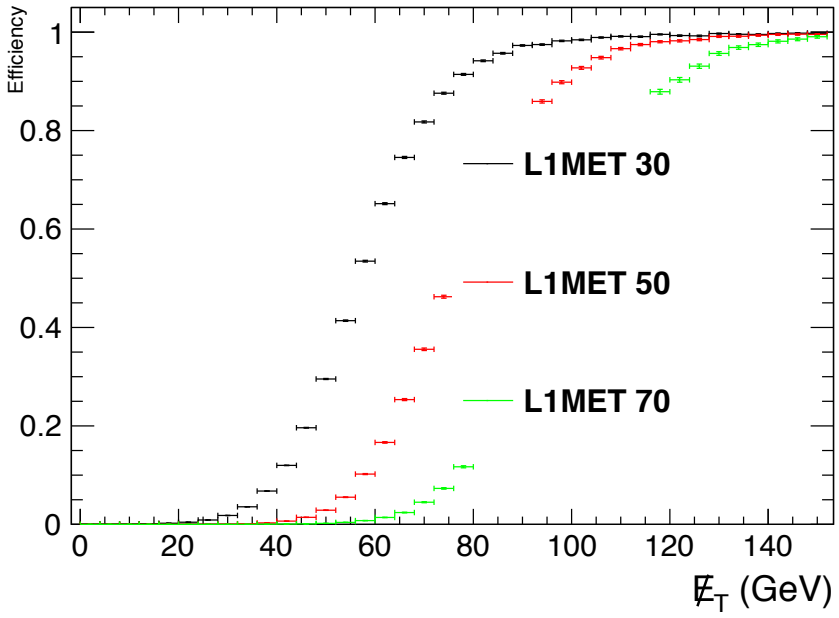

Figure 5.11: Performance of the Level-1 $\not{E}_T$ triggers, preselecting on HLT_IsoMu24. The fit results are listed in Table 5.6.

Trigger	σ	μ
L1_MET30	13.53	57.65
L1_MET50	14.09	76.02
L1_MET70	16.51	97.37

Table 5.6: Results of an error function fit to the turn on curves for Level-1 hadronic energy sum ($\not{E}_{\mathrm{T}}$) triggers in run 2011B. Preselected on an Isolated Muon trigger.

5.3 Level-1 Trigger Pile-up Mitigation

Due to the lack of a requirement of a jet seed threshold, soft non-collimated jets, such as those expected in a high pile up environment are found. Trigger decisions are then made using these pile up jets.

This is less of a problem for the single jet triggers which have a high P_T threshold. However the H_{T} triggers, where $H_{\mathrm{T}} = \sum_{jets} E_T^{jet}$ and the requirement of $E_{\mathrm{T}}{}^{jet} \geq 10$ GeV is made, see a large increase in rate due to pile-up, this is due to the low energy threshold required for a jet to be added to the H_{T} sum.

To counteract the effect of pile up on trigger rate we study the effects of requiring a jet seed threshold on the rate and efficiency of the individual jet and H_{T} triggers.

Figure 5.2 depicts 3×3 trigger regions, each of which are built from 4×4 trigger towers. In this case the central region is the jet seed. The proposed change would require there to be a threshold energy in the seed region.

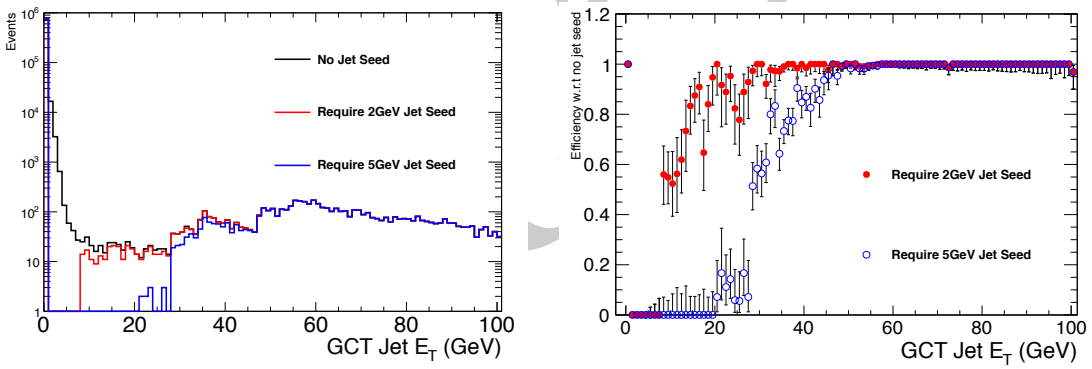

(a) GCT internal uncorrected jet E_{T} distributions for the same events with a 0, 2 or 5 GeV seed requirement.

(b) Efficiency of applying a requirement of 2 or 5 GeV GeV with respect to no requirement.

Figure 5.12: Effect of requiring a jet seed threshold on GCT internal jets.

The study of using jet seed thresholds of 2 and 5 GeV is presented. Figure 5.12 shows how the different threshold requirements effect the rank of the internal GCT jets. The effect is to remove all jets below 2(5) GeV and to cut out jets from the low end of the distribution. From Figure 5.12(b) it is possible to see the point beyond which the requirement of a jet seed has no effect. For a cut of 2 GeV jets above an uncorrected E_{T} of ≈ 35 GeV are not effected, for a seed threshold of 5 GeV jets above an uncorrected E_{T} 55 GeV are not effected.

Table 5.7: Summary of rate reduction during low pile up conditions.

Trigger	% of rate taken with 2 GeV requirement	% of rate taken with 5 GeV requirement
L1_HTT100	$98.6 \pm 11.6\%$	$97.9 \pm 11.6\%$
L1_QuadJet38	$100.0 \pm 0.0\%$	$85.3 + 6.2 - 8.7\%$
L1_Jet50	$100.0 + 0.0 - 12.3\%$	$85.7 + 9.1 - 15.8\%$

5.3.1 Effect on trigger rates

The effects of applying a seed threshold are quantified in terms of the level of rate reduction in the Level-1 hadronic triggers. Three triggers are studied, they are:

- L1_SingleJet50 - Level one trigger requiring at least one jet with a corrected $E_{\mathrm{T}} \geq 50$ GeV.
- L1_HTT100 - Level one trigger requiring $H_{\mathrm{T}} \geq 100$ GeV.
- L1_QuadJet38 - Level one trigger requiring at least four jets in the event with $E_{\mathrm{T}} \geq 38$ GeV.

5.3.2 Low Pile Up

A small effect on trigger rates in the low pile up scenario is expected due to the majority of energy deposited in the calorimeters coming from hard scattering.

Table 5.7 shows the rate reduction of requiring a 2 or 5 GeV seed threshold with respect to requiring no seed threshold.

5.3.3 High Pile Up

Pile up is expected to add a small quantity of energy to the entire calorimeter system, this energy comes in the form of soft non-collimated jets. These objects are then not reconstructed if the topological cut of applying a seed threshold is required.

Table 5.8 shows the rate reduction of requiring a 2 or 5 GeV seed threshold with respect to requiring no seed threshold in high pile up conditions.

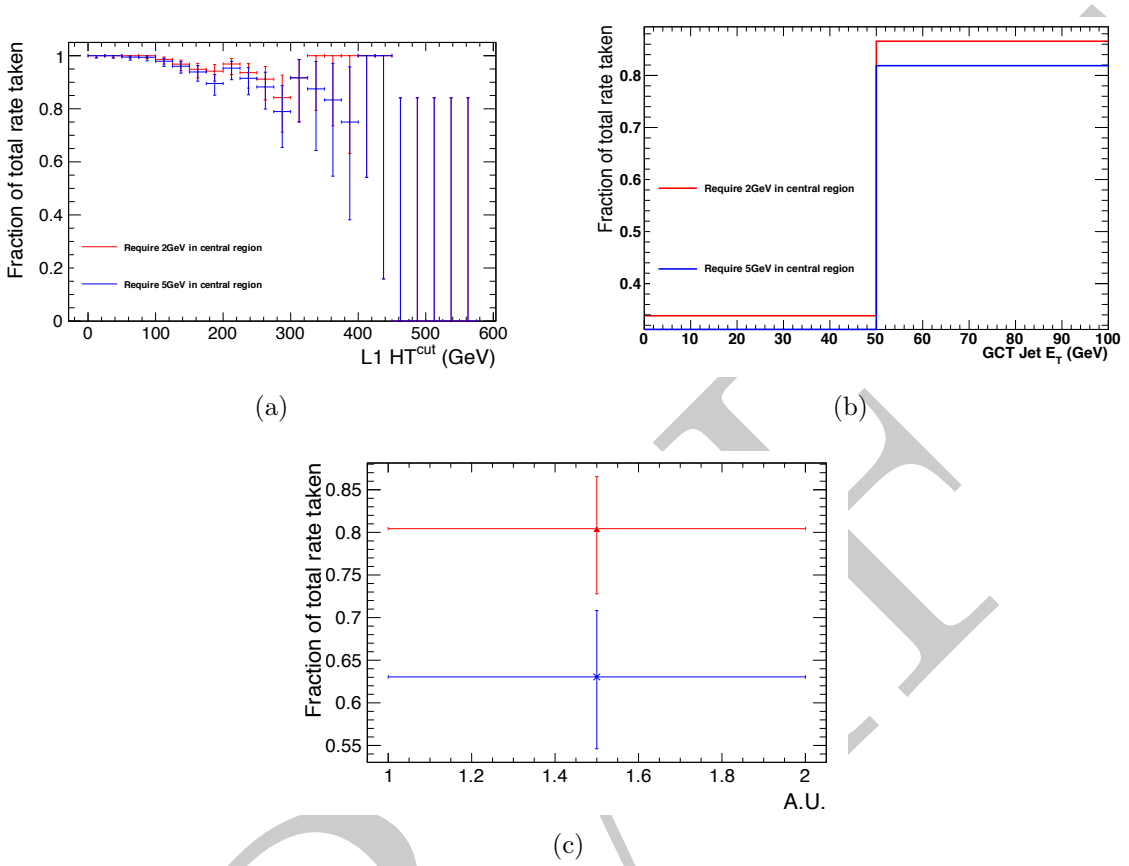

Figure 5.13: Rate reductions for various Level-1 algorithms when applying a 2,5 GeV seed tower requirement, in low pile up conditions. Figure (a) shows the rate reduction for H_{T} triggers at low pile up in cut steps of 25 GeV. Figure (b) shows the rate reduction for jets with in $|\eta| < 3.$ and $p_{\mathrm{T}} > 50$ GeV. Figure (c) shows the rate reduction for a quad jet trigger, with jet $|\eta| < 3.$ and $p_{\mathrm{T}} > 38$ GeV.

Table 5.8: Summary of rate reduction during high pile up conditions.

Trigger	% of rate taken with 2 GeV requirement	% of rate taken with 5 GeV requirement
L1_HTT100	$60.4 \pm 5.7\%$	$0.67 + / - 0.67\%$
L1_QuadJet38	$71.4 + 18.2 - 25.9\%$	$57.1 + 22.3 - 24.8\%$
L1_Jet50	$100.0 + 0.0 - 7.7\%$	$73.9 + 9.8 - 12.3\%$

5.3.4 Effect on trigger efficiency

Section 5.3.1 shows that requiring a jet seed threshold substantially reduces the trigger acceptance rate at in high pile up conditions.

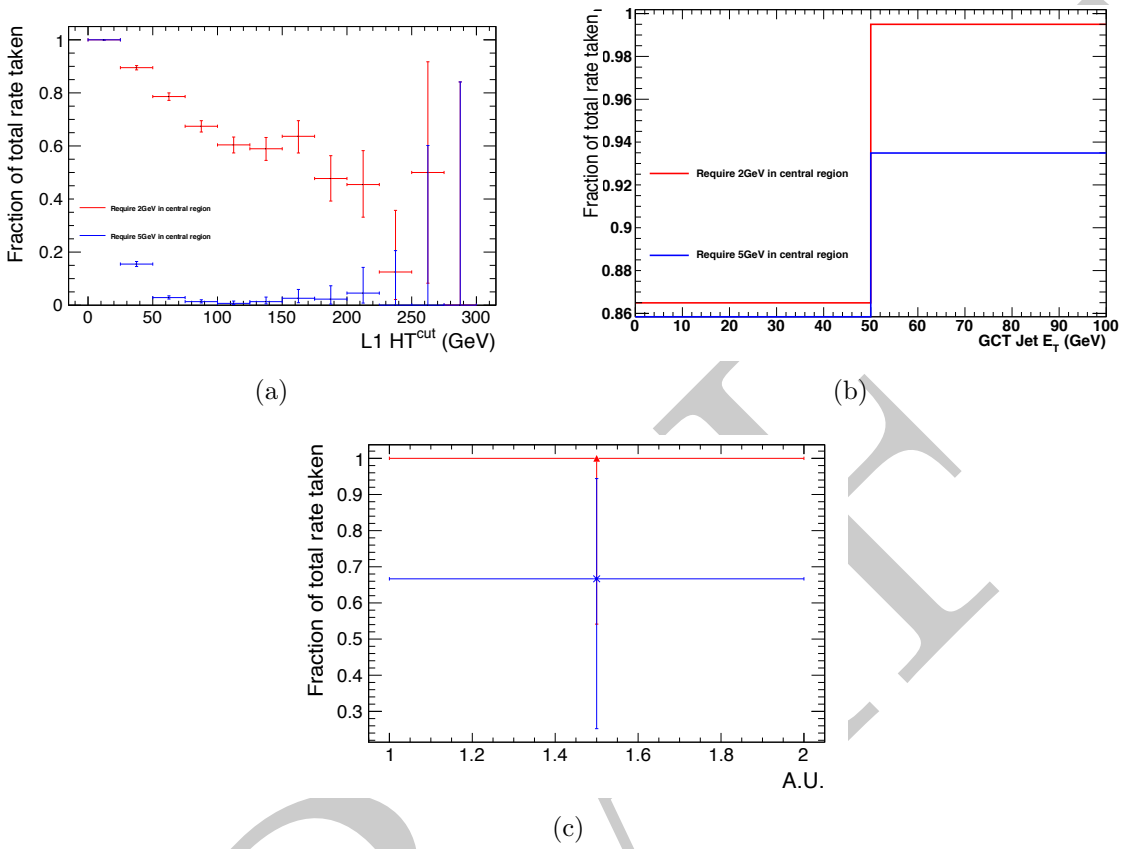

Figure 5.14: Rate reductions for various Level-1 algorithms when applying a 2,5 GeV seed tower requirement, in high pile up conditions. Figure (a) shows the rate reduction for H_{T} triggers at high pile up, in cut steps of 25 GeV. Figure (b) shows the rate reduction for jets with in $|\eta| < 3.$ and $p_{\mathrm{T}} > 50\,\mathrm{GeV}$. Figure (c) shows the rate reduction for a quad jet trigger, with jet $|\eta| < 3.$ and $p_{\mathrm{T}} > 38\,\mathrm{GeV}$

However the aim of requiring a jet seed is to reduce rate, but not at the cost of physics. In this section we look at the effects of requiring a seed threshold, whilst requiring some loose, generic offline selection on the hadronic objects.

The change in efficiency is measured under low pile up conditions where the least extra energy added to the event. This gives a worse case estimate of the effect of requiring a jet seed on the offline efficiency.

Each offline reconstructed calorimeter jet must adhere to the following quality criteria:

- Pass loose calorimeter ID
- $p_{\mathrm{T}} \geq 30$ GeV.
- $|\eta| \leq 3.0$.

- Matched to a Level-1 jet with $\Delta R \leq 0.5$.

Where loose calorimeter ID is defined as; Electro-Magnetic fraction > 0.01, fraction of energy in the Hybrid Photo Diodes < 0.98 and the number of n90hits > 1.

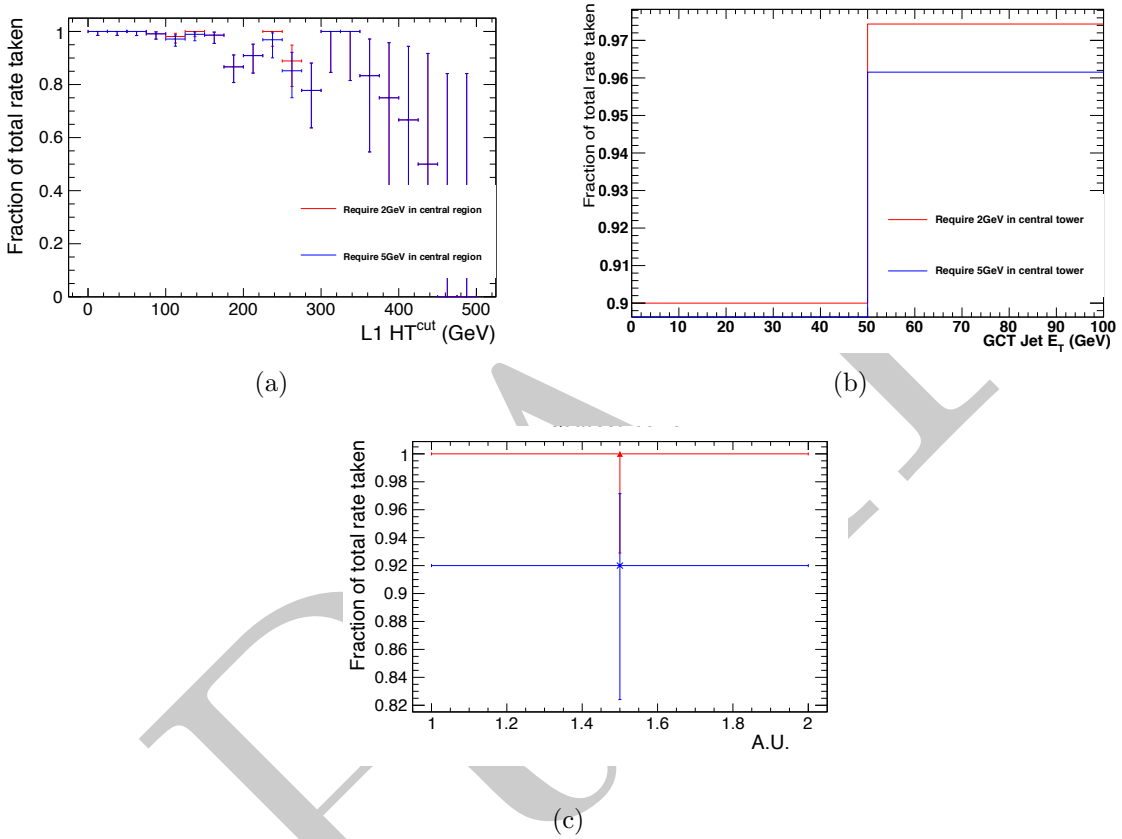

Figure 5.15: Efficiency reductions for various Level-1 algorithms when applying a 2 or 5 GeV seed tower requirement, in low pile up conditions. Figure (a) shows the efficiency reduction for H_{T} triggers at low pile up in cut steps of 25 GeV. Figure (b) shows the efficiency reduction for jets with in $|\eta| < 3.$ and $p_{\mathrm{T}} > 50\,\mathrm{GeV}$. Figure (c) show the efficiency reduction for a quad jet trigger, with jet $|\eta| < 3.$ and $p_{\mathrm{T}} > 38\,\mathrm{GeV}$.

Efficiency of H_{T} Triggers Figure 5.15(a) shows the acceptance reduction after applying the two jet seed thresholds. The distribution is the cumulative number of events passing a cut of $L1HT^{cut}$ in bins of 25 GeV. Due to H_{T} being the scalar sum of the jet p_{T}'s in the event the value of Level-1 H_{T} is reduced as jets are removed from the calculation. To preserve efficiency the Level-1 trigger threshold will have to be reduced. Comparing figures 5.13(a) and 5.15(a), if the trigger threshold is reduced to 75 GeV an efficiency of $\geq 95\%$ can be maintained whilst reducing the trigger rate by $\approx 2\%$ when

requiring a 2 GeV seed threshold and reduced by $\approx 3\%$ when requiring a 5 GeV seed threshold. When comparing to the high pile up rate reduction in figure 5.14(a) it is shown that the trigger rate can be reduced by $\approx 20\%$ when requiring a 2 GeV seed threshold and reduced by $\geq 99\%$ when requiring a 5 GeV seed threshold.

Efficiency of Jet Triggers Figure 5.15(b) shows the change in acceptance of jets in low pile up conditions when the two seed thresholds are required. The effect is on the order of a few percent for each of the thresholds. Requiring a 2 GeV seed reduces the efficiency for jets above 50 GeV by $\approx 2.5\%$, whilst requiring a 5 GeV seed reduces the efficiency of the same jets by $\approx 4\%$.

Efficiency of MultiJet Triggers Figure 5.15(c) shows that the effect of requiring a seed threshold of 2 GeV has no effect on the efficiency of the quad jet 38 GeV trigger and requiring a seed threshold of 5 GeV reduces the efficiency of the quad jet 38 trigger by 8%. The change in rate is dramatic in high pile up conditions where for a 2 GeV seed threshold the rate is reduced by $\approx 30\%$ and by $\approx 40\%$ when requiring a 5 GeV seed. However it is to be noted that the sample where this measurement has been made is of limited size, inferring a reasonably large statistical uncertainty.

5.3.5 Summary

The effects of requiring a jet seed have been studied using the Level-1 trigger emulator on high and low pile-up samples. The studies show that requiring a jet seed of 5 GeV greatly reduces the rate of the H_{T} and Multi Jet triggers in high pile up conditions, whilst not adversely effecting the data taking efficiency of these triggers.

The cross section of L1_HTT150 has been measured with and with out the addition of a jet seed threshold of 5 GeV as shown in Figure 5.16. Ideally the trigger cross section would be independent of the instantaneous luminosity and pile up, Figure 5.16 shows that the addition of a 5 GeV seed threshold reduces the dependance on instantaneous luminosity of the trigger cross section.

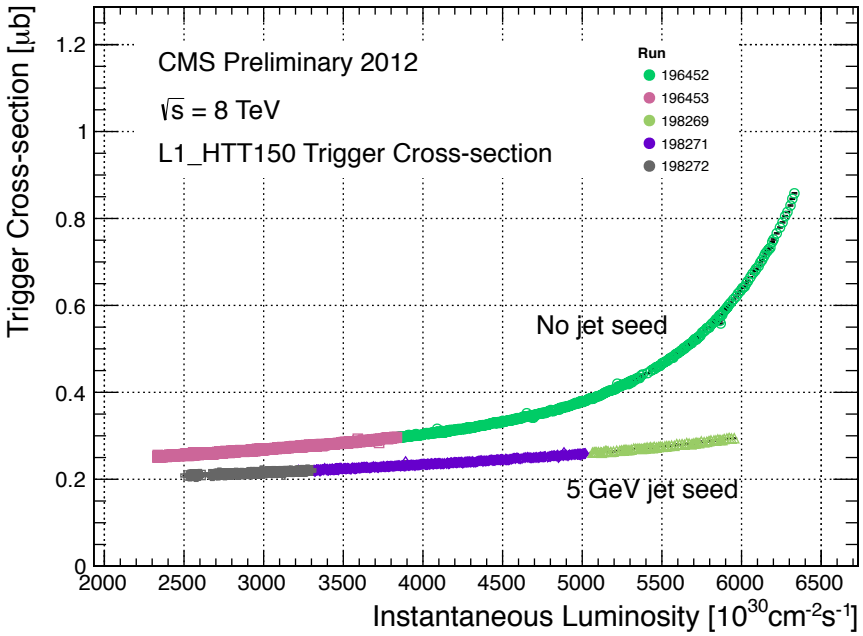

Figure 5.16: Trigger cross section as a function of number of pile up interactions. Showing that applying a 5 GeV jet seed threshold dramatically reduces the quadratic dependance of cross section on the number of pile up interactions

Chapter 6

High level triggers for the α_T analysis.

Chapter 7

The α_T analysis

In this chapter we discuss the main analysis performed as the subject of this thesis. For the theoretical motivations of this search please see Chapter 2. The analysis is based on the full 2011 data set which is made up of $5\,\text{fb}^{-1}$ of 7 TeV data. However $5\,\text{fb}^{-1}$ of the 2012 8 TeV is looked at to measure the performance of the upgraded α_T HLT paths.

7.1 The Problem

If Supersymmetry or some other beyond the standard model theory is to provide a yet undiscovered dark matter candidate, it is predicted that this candidate will interact via the weak nuclear force only. This gives a decay topology involving missing energy in the form of the dark matter particle escaping the detector. Due to the nature of interactions at the L.H.C, these particles would be produced at the end of a decay chain of heavy particles that interact strongly, giving a final topology involving hadronic objects which are classified as jets for the purpose of analysis and missing energy. There are several standard model processes that mimic this final state.

By far the largest of these backgrounds comes from QCD multi jet events where fake missing energy is introduced either from failures in reconstruction, or stochastic fluctuations in the calorimeter systems. **FIXME: expand on this - E /sqrt E has non gaussian tails. Figures of jets falling below threshold, missed jets etc. probably from some jet-met paper.** However due to the theoretical errors on the QCD production cross section predicting the number QCD background events from Montecarlo simulation is not possible. A secondary QCD background also exists, where due to the requirement of a jet E_{T} threshold, multiple jets fall under threshold by 1-5

GeV, this causes a balanced event to look unbalanced as the jets under threshold are no longer considered. The solution is then to devise a kinematic cut that removes these events from the signal selection.

The second major background comes from standard model electro-weak decays and is irreducible. The electro-weak decays that form the back ground are W $\rightarrow \tau\nu$ + Jets, where the τ is reconstructed as a jet, or the lepton fails the identification required for the dedicated lepton vetoes, Z $\rightarrow \nu\overline{\nu}$ + Jets is completely irreducible. These are generally di-jet topologies. At higher jet multiplicities top quark production followed by semi-leptonic top decay accounts of the largest background. These backgrounds are predicted using a well understood control sample this is fully explained in Section 7.4.

The final background source is that introduced by detector failure or electronic noise induced by the movement of the L.H.C proton beam. Approximately 1% of the ECAL read out is not available in offline event reconstruction, this provides a source of fake missing energy.

7.2 The α_T variable.

α_T is inspired by Ref [10] and was expanded to transverse multi jet topologies by members of the CMS collaboration in Refs [5, 6]. The purpose is to provide a variable that can be cut on to eliminate QCD from the final selection. To do this the inherent balance of the QCD system is exploited.

For di-jet systems α_T is defined as:

$$\alpha_T = \frac{E_{\mathrm{T}}^{j_2}}{M_T} \tag{7.1}$$

where $E_{\mathrm{T}}{}^{j_2}$ is the transverse energy of least energetic of the two jets and M_T is defined as:

$$M_T = \sqrt{\left(\sum_{i=1}^{2} E_{\mathrm{T}}^{j_i}\right)^2 - \left(\sum_{i=1}^{2} p_x^{j_i}\right)^2 - \left(\sum_{i=1}^{2} p_y^{j_i}\right)^2} \tag{7.2}$$

For a perfectly measured di-jet system with $E_{\mathrm{T}}{}^{j_1} = E_{\mathrm{T}}{}^{j_2}$, where the jets are opposite in ϕ $\alpha_T = 0.5$, for events with back to back jets where one is miss-measured $\alpha_T < 0.5$. However the majority of signals predict many jets in the final state. α_T can be generalised to work with n-jets in the flowing way. The variables H_{T}, $\not{H}_{\mathrm{T}}$ and ΔH_{T} are constructed:

$$H_{\mathrm{T}} = \sum_{i=0}^{n\ jets} E_{\mathrm{T}}^{jet_i} \tag{7.3}$$

$$\not{H}_{\mathrm{T}} = \left| \sum_{i=0}^{n\ jets} \vec{p}_T^{\,jet_i} \right| \tag{7.4}$$

for jets above some predefined threshold E_{T} which is common for all jet based quantities. The multi jet system is reduced to a pseudo di-jet system by forming two large jets. The individual jet E_{T}'s are summed, with the final configuration being chosen to have the minimum difference in energy (ΔH_{T}) between the pseudo jets. This simple clustering criteria provides the best separation between miss-measured events and those with real $\not{E}_{\mathrm{T}}$.

α_T is then defined as:

$$\alpha_T = \frac{H_{\mathrm{T}} - \Delta H_{\mathrm{T}}}{2\sqrt{H_{\mathrm{T}}^2 - \not{H}_{\mathrm{T}}^2}} \tag{7.5}$$

Figure 7.1 shows the α_T distribution for both data and simulated background samples. The QCD multi jet background is negligible above an α_T value of 0.55, where as the standard model processes which involve real $\not{E}_{\mathrm{T}}$ exist at all possible values of α_T. Values of α_T in the range $0.5 < \alpha_T < 0.55$ arise in multi jet QCD due to jets falling below threshold or large stochastic fluctuations. It is to be noted that the discrepancy between data and simulation for $\alpha_T \leq 0.55$ is due to no trigger emulation being applied to the simulated background samples.

7.3 High Level triggers for the α_T analysis

The CMS trigger system has been discussed in detail in Section 3.1 and Chapter 5, however details of analysis specific trigger paths were not discussed. During 2011 the first α_T specific trigger was designed and deployed online. The trigger was then upgraded for the higher luminosity and energy conditions of the 2012 data taking period.

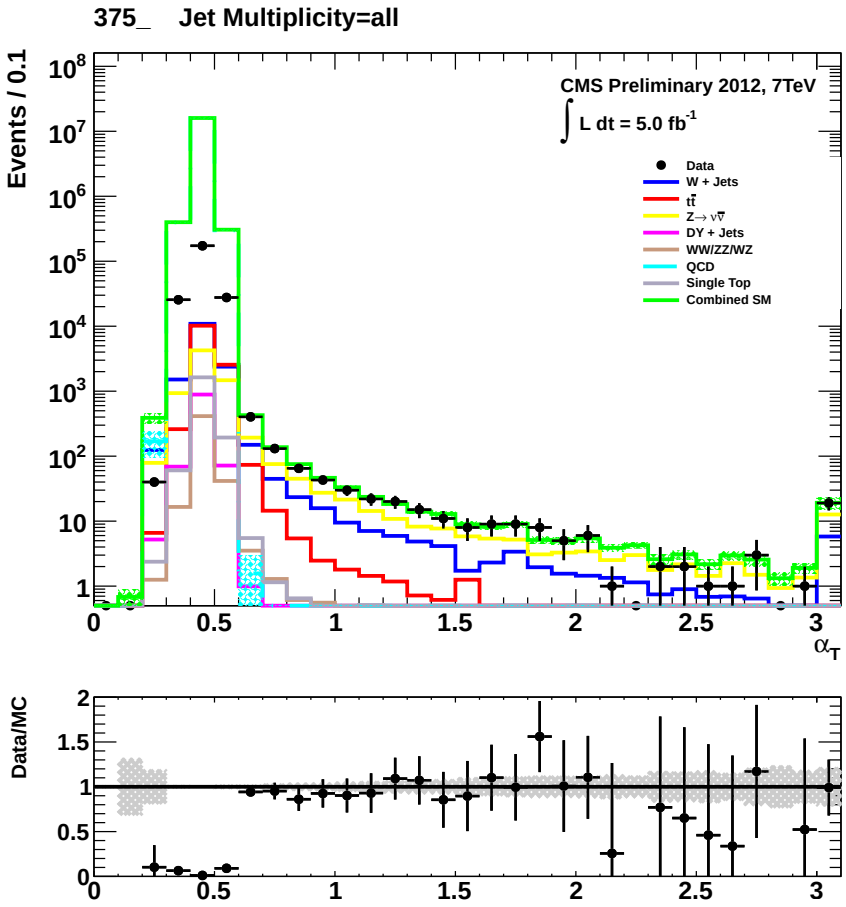

Figure 7.1: α_T distribution for background and data. Trigger emulation is not applied in the simulated background which leads to the discrepancy in the region $\alpha_T \leq 0.55$. The QCD multi-jet background is reduced to less than one event.

7.4 Electro-Weak background prediction

Chapter 8

Conclusion

1

Bibliography

[1] T Åkesson. The ATLAS experiment at the CERN Large Hadron Collider - CERN Document Server. *Particles*, 1999.

[2] B Alessandro, F Antinori, J Belikov, and C Blume. ALICE: Physics performance report, volume II. *Journal of Physics G: Nuclear and Particle Phyiscs*, January 2006.

[3] Michael Benedikt, Paul Collier, V Mertens, John Poole, and Karlheinz Schindl. *LHC Design Report*. CERN, Geneva, 2004.

[4] CMS Collaboration. The Trigger and Data Acquisition Project Technical Design Report, Volume 1, The Level-1 Trigger. *CERN/LHCC 2000-038, CMS TDR 6.1*, 2000.

[5] CMS Collaboration. SUSY searches with dijet events. Technical report, 2008.

[6] CMS Collaboration. Search strategy for exclusive multi-jet events from supersymmetry at CMS. Technical report, 2009.

[7] M Friedl, N Frischauf, T Bauer, T Bergauer, W Waltenberger, A R Knapitsch, C Irmler, I Kratschmer, W Treberer-treberspurg, B Rahbaran, V Innocente, T Camporesi, S Gowdy, L Malgeri, A Marchioro, L Moneta, W Weingarten, M Giunta, M Rovere, A Bonato, A C Spataru, S Zhang, A Perieanu, N Heracleous, H K V Reithler, B Philipps, M K Merschmeyer, C A Heidemann, H Geenen, Y Kuessel, E Kuznetsova, J Olzem, A Bethani, L Calligaris, R Walsh bastos rangel, T M M Dorland, G Quast, A H Dierlamm, I Katkov, R M Ulrich, F M H Stober, C Barth, X Mol, A Kornmayer, F Matorras, A Calderon tazon, A Lopez garcia, J A Brochero cifuentes, M J Bercher, M Haguenauer, Y Sirois, C M Mironov, P Depasse, L Sgandurra, G P Heath, Z Meng, D A Hartley, N I Geddes, S Quinton, I R Tomalin, K Harder, V B Francis, Z Zhang, T Geralis, D Loukas, I Topsis giotis, G Bencze, S T Hernath, I Szeberenyi, S Banerjee, S Singh, A Colaleo, G P Maggi, M Maggi, F Loddo,

R Campanini, I D'antone, C Grandi, L Guiducci, M Gulmini, S Fantinel, P Meridiani, K K Joo, S Song, J Rhee, E Won, M Jo, H Kim, D H Kim, G N Kim, J E Kim, T Son, W M Dominik, K Bunkowski, J C Rasteiro da silva, J Varela, A Alves, V Sulimov, A Vorobyev, V Murzin, S Lukyanenko, G Mesyats, V Postoev, A Pashenkov, A Solovey, S Troitsky, N Lychkovskaya, G Safronov, A Fedotov, K Olimov, M Fazilov, A Umaraliev, I Dumanoglu, N M Bakirci, C Dozen, M Zeyrek, M Yalvac, S Ozkorucuklu, K Sevim, Y Chang, W T Lin, S Bahinipati, K A Biery, E E Gottschalk, K Maeshima, T Kramer, S W L Kwan, S J Murray, L Taylor, N Mokhov, J M Marraffino, S Mrenna, V Yarba, B Banerjee, V D Elvira, D C Hare, B Holzman, F X Yumiceva del pozo, W Dagenhart, C L Dumitrescu, S C Ryu, B J Kilminster, J K Adelman-mc carthy, V E Bazterra, I Bucinskaite, P E Karchin, J R Incandela, M D'Alfonso, R Rossin, C A West, J L Gran, G Zilizi, P P Raics, A Bhardwaj, M Naimuddin, A Kumar, N Smiljkovic, C P De oliveira martins, M Petek, A Vercosa custodio, E J Tonelli manganote, M T Narjanen, P Graehling, F Blekman, J M Keaveney, S Blyweert, N van Remortel, X J Janssen, D Druzhkin, M Bansal, A Aleksandrov, M F Shopova, T R Fernandez perez tomei, C Krug, A A Shinoda, T V Rohe, P Arce, M Daniel, J J Navarrete marin, I Redondo fernandez, A Guirao elias, J Santaolalla camino, J Lottin, P Gras, F Kircher, B Levesy, A Payn, A K Nayak, V Bhatnagar, C Randieri, M Bruzzi, O Starodubtsev, A Tropiano, D Piccolo, C Sciacca, S Meola, A Saccomanno, M Esposito, P Azzi, E Conti, S Lacaprara, M Margoni, M Sgaravatto, N Pozzobon, P Torre, B Checcucci, L Fanò, S Taroni, A Lucaroni, F Romeo, G Bagliesi, M A Ciocci, A Giassi, T Boccali, S Arezzini, A Rizzi, G Broccolo, D Dattola, C Mariotti, A Ballestrero, E Camacho-Pérez, R Magaña-Villalba, J Martínez-Ortega, M Górski, G Wrochna, M J Bluj, A Zarubin, M Nozdrin, V Ladygin, A Golunov, A Sotnikov, N Evdokimov, I Lokhtin, A Ershov, N Tyurin, S Akimenko, V Talov, N Belikov, A Ryazanov, G W Hou, Y Chao, J Alwall, X Shi, D R Wood, D C Baumgartel, J Zhang, P D Luckey, K C Sumorok, G Gomez ceballos retuerto, S H Jaditz, G S Stephans, T Ma, P J Lehtonen, M H Chan, I J Moult, R A Ofierzynski, A Pozdnyakov, B L Pollack, P B Padley, A H Adair, W J Clarida, E Tiras, G Cerizza, M Pieri, V A Sharma, M W Lebourgeois, M Norman, F Golf, M J Murray, J L S Bowen, K Buterbaugh, M Sharma, J Bunn, H Newman, M Gataullin, M Spiropulu, J Veverka, S D Thomas, K J Rose, S M Panwalkar, A Calamba, Z Xie, J S Werner, A M Zuranski, A Ferapontov, E M Laird, G Kukartsev, Z Mao, S J Wimpenny, S Gleyzer, M G Weinberg, V Veeraraghavan, and J... Bochenek. CMS - The Compact Muon Solenoid. January 1996.

[8] J Marrouche and others. Commissioning the CMS Global Calorimeter Trigger. *CMS*

IN, 2010/029, 2010.

[9] J Rademacker. LHCb: Status and Physics Prospects. *Arxiv preprint hep-ex*, January 2005.

[10] Lisa Randall and David Tucker-Smith. Dijet Searches for Supersymmetry at the LHC. *arXiv*, hep-ph, January 2008.

[11] C Wulz. The CMS experiment at CERN. *cdsweb.cern.ch*.